Materials and Structures (2025) 58:91
https://doi.org/10.1617/s11527-025-02598-w

ORIGINAL ARTICLE

# Systematic study on mix design optimization and on fresh properties of grouts containing crystalline admixtures

**Suelen da Rocha Gomes · Isabel Santacruz · Luis Sánchez · Mercedes Sánchez Moreno**

Received: 12 September 2024 / Accepted: 6 February 2025 / Published online: 14 March 2025


**Abstract** Crystalline admixtures (CA) are often proposed as admixtures for improving self-healing ability of cement-based materials. While significant progress has been made in smart concretes and mortars, the application of self-healing technology in grouts remains underexplored. The design of a grout is complex because any change in its composition will have a significant effect on its properties, especially in the fresh state. This work analyses the effect of the incorporation of the CA on the production of a self-repairing grout. The study focuses on the effects of CA on the fresh and hardened properties of grouts. A comprehensive analysis of grout design highlights the influence of critical parameters such as water/binder (*w*/*b*) and sand/binder (*s*/*b*) ratios, supplementary materials (fly ash and limestone), and superplasticizer (SP) dosages. Formulating a grout with CA requires greater efforts to achieve an optimal balance between the fresh and hardened properties. CA affected particle dispersion, stability and consistency of grouts. Designing grouts (with and without CA) with similar fluidity required higher SP dosages, which improved the viscosity and delayed the setting time. CA accelerates the hydration of $C_3S$ and $C_3A$ hydrates formation and shortens the induction period, but when combined with SP, its contribution is reduced. Compressive strength of grout with CA were higher than reference at all tested ages.

**Keywords** Grout · Mix design · Crystalline admixtures · Workability

## 1 Introduction

When designing a cement-based grout, expertise is essential in grout formulation due to the wide range of applications and numerous parameters (e.g., composition, *w*/*b* and *s*/*b* ratios, mixing conditions, among others) that must be considered in an overall design framework [1–3]. Although there are some research reports and standards [4–7], many do not specify the exact properties a grout must exhibit nor detail the particularities of its formulation, and most grouts are produced based on empirical practices.

**Supplementary Information** The online version contains supplementary material available at https://doi.org/10.1617/s11527-025-02598-w.

S. da Rocha Gomes (✉) · L. Sánchez · M. Sánchez Moreno (✉)
Departamento de Química Inorgánica e Ingeniería Química, Instituto Químico para la Energía y el Medio Ambiente (IQUEMA), Universidad de Córdoba, Córdoba, Spain
e-mail: sdrocha@uco.es

M. Sánchez Moreno
e-mail: msmoreno@uco.es

I. Santacruz
Departamento de Química Inorgánica, Cristalografía y Mineralogía, Universidad de Málaga, Málaga, Spain

Workability is an essential property and is usually measured through rheological measurements, setting time and flow measurements (flow time and flow table spreading) [2]. As fluidity is a primary characteristic of grout, it requires a balanced *w/b* ratio to maintain the grout performance. A high *w/b* ratio improve fluidity, but can also increase bleeding and porosity, impairing cohesion and leading to sedimentation and segregation [8]. When bleeding is high, this also results in uneven settling and strength losses [9–12]. Minimizing bleeding is important for achieving optimal grout performance. Some papers indicated that a maximum of 5% of bleeding is acceptable [13, 14].

To address workability issues, chemical admixtures (as superplasticizers (SP)) and some supplementary cementitious materials (SCM) are often incorporated [15–22]. In this study, part of the cement was replaced with fly ash (FA) as it was reported as an agent to improve the workability due to a lubrication effect [23], in addition to decreasing the yield stress [24] and, reducing the apparent viscosity [25]. Limestone (LS) was also used as it can improve the microstructure and may modify the rheological properties. Although it is considered an inert filler, LS can alter the hydration kinetics of cement and the morphology of hydration products [26, 27]. Depending on the grain size distribution of fine aggregates, the bleeding rate and compressive strength can be improved [28].

Grouts can exhibit fluid, plastic or flowable consistencies, with flow tests (flow table spread and flow time) frequently used to measure this property [7, 29–31]. Generally, grout stability is proportional to its viscosity and inversely proportional to fluidity. Therefore, studying its rheological behavior is essential to anticipate and mitigate issues like sedimentation, segregation and filtration [32–36].

Usually, cementitious grouts are described as non-Newtonian fluids. The rheological models provide theoretical descriptions of the rheological behavior and are not absolute rules. In a real scenario, the material may demonstrate more than one behavior across different shear rate ranges.

For grouts, both the yield stress (related with the cohesion forces between particles) and viscosity are important parameters because they provide information on the stability and injectability. Some grouts follow the simplest rheological behavior, called Bingham model, that obey Eq. 1, where $\tau$ is the measured shear stress (Pa) at a shear rate ($s^{-1}$) of $\dot{\gamma}$, $\tau_0$ is the (dynamic) yield stress (Pa) and $\mu_p$ is the plastic viscosity (Pa.s).

$$\tau = \tau_0 + \mu_p * \dot{\gamma} \tag{1}$$

As Bingham does not consider the nonlinearity of the flow curve in certain shear rate ranges, grouts can be characterized by more complex models, such as the Casson or Herschel-Bulkley models. In the Herschel–Bulkley model, shown in Eq. 2, $\tau$ is the shear stress (in Pa), $\dot{\gamma}$ is the shear rate (in $s^{-1}$), $\tau_0$ is the yield stress (in Pa), $K$ is the consistency index (in Pa $s^n$) and $n$ is the exponent (flow behavior index). Values of $n<1$ are related to a shear thinning behavior (viscosity decreases by increasing the shear rate), and $n>1$ with a shear thickening behavior (viscosity increases by increasing the shear rate), and when $n=1$, this model is equivalent to the Bingham model.

$$\tau = \tau_0 + \mathrm{K} * \dot{\gamma}^n \tag{2}$$

Grouts are also susceptible to cracking that impairs their durability (as cracks can expand and propagate). In this context, self-healing materials have emerged as an option to enhance the durability [37]. Cement inherently exhibits a degree of self-healing (classified as autogenic healing) limited to repairing cracks smaller than 100 microns. For cracks exceeding this width, autonomic healing is required (repairing depends on the addition of other materials). A variety of design strategies can provide self-healing ability [38] and addition of CA is one of them [39–43].

In particular, the CA used in this work is a PRAH type (permeability reducing admixture used for concrete in non-hydrostatic conditions). According to ACI 212.3R-10 report [44], the proposed reaction mechanism of PRAH type is similar to the formation of C-S–H, that is, the active ingredients of the CA react with water and cement particles to form C-S–H and/or pore-blocking precipitates that are deposited in the capillaries and microcracks. The reaction mechanism is represented in Eq. 3:

$$\begin{aligned} &3\,\mathrm{Ca} - \mathrm{SiO_2} + \mathrm{M_xR_x} + \mathrm{H_2O} \rightarrow \\ &\mathrm{Ca_xSi_xO_xR} - \left(\mathrm{H_2O}\right)_x + \mathrm{MxCaRx} - \left(\mathrm{H_2O}\right)_x \end{aligned} \tag{3}$$

There is no consensus on the impact of CA on workability as both improvements and worsening were reported [39, 41, 45–48].Publications on the design of grouts with CA is scarcely reported. Wang et al. [49] reported that CA did not alter the slump

but increased both long-term compressive strength and modulus of elasticity. Zheng et al. [50] did not observed significant changes in setting time and in viscosity but registered a slight increase in compressive strength.

Due to the limited studies detailing grout compositions with CA, this work analyzes the influence of CA on grouts. First, the study discusses the production of grouts (with and without CA) analyzing the flow and bleeding results. Two *w*/*b* ratios (0.45 and 0.6) and two *s*/*b* ratios (0.9 and 1.2) were considered starting points for the grout design. The tests began with the preparation of grouts containing only cement, sand and water to identify how these parameters would affect the stability (bleeding measurements) and consistency (flow measurements) of the mixtures. The grouts designed were thought to be fluid in terms of Marsh flow time (less than 1 min in continuous flow) presenting bleeding as low as possible. It is important to note that qualitative results from Marsh flow tests can give a false-positive result, as many formulations may flow perfectly through the cone despite being clearly unstable due to high bleeding content. Thus, flow results must be interpreted together with bleeding rate data. Additionally, when the optimal formulations were found, they were characterized by the initial setting-time and early hydration process (ultrasonic pulse measurements and isothermal calorimetry), rheological behavior and compressive strength.

The design process was carried out through a series of experiments, establishing a benchmark that allows other workers/researchers to compare and identify gaps and potential improvements to make performance comparable.

## 2 Methodology

### 2.1 Design of grout mixtures: optimization of fresh properties (flow and bleeding)

The grout preparation was divided into two stages: in the first stage, an initial study was undertaken to identify the most suitable formulation, focusing on the proportions of components, consistently maintaining a CA dosage of 3% (by weight of binder), as recommended by the manufacturer. This preliminary study analyzed the effects of two key parameters on fluidity and bleeding: the *w*/*b* ratio (0.45 and 0.6) and the *s*/*b* ratio (0.9 and 1.2). The primary criterion aimed for a stable mix with minimal bleeding and a flow time as consistent as possible between the grouts with and without CA. To optimize workability and stability, several approaches were tested, including adding or substituting cement with FA, adding or substituting sand with LS and incorporating SP. The design process prioritized the formulation of grouts containing CA. Once these were optimized, a reference grout with matching flow time was developed. This reference formulation was designed to obtain similar performance in terms of fluidity, with minimal bleeding.

After finalizing both formulations, the second stage focused on further evaluations to better understand the effects of CA on the fresh and hardened properties of the grouts.

### 2.2 Materials

Grouts were prepared using Portland cement I 42.5 R (according to European standard EN 197–1), class F FA, siliceous standard sand EN 196-1 (Normensand GmbH), LS (provided by Votorantim Cimentos), MasterCast 228 (beta naphthalene-based SP provided by Master Builder Solutions), defoamer (a solid additive provided by Master Builder Solutions) and Penetron Admix ( provided by Penetron Italia Srl). All components used were solid and were stored at controlled temperature of $24 \pm 1$ °C.

The chemical composition of the cement, FA, LS and CA obtained by X-Ray Fluorescence (XRF) is presented in Table 1. All the raw materials are rich in CaO and $SiO_2$ except FA which is rich in $SiO_2$ and $Al_2O_3$. CA and cement have similar $CaO/SiO_2$ ratio, 3.75 and 3.72, respectively. It is also observed that CA has a higher percentage of MgO (4.89%).

A diffractometric analysis (XRD) is presented in Fig. 1. The XRD pattern of CEM I 42.5R revealed the presence of the main phases: $C_3S$ (alite), $C_2S$ (belite), $C_3A$ (tricalcium aluminate), $C_4AF$ (ferrite) and gypsum in agreement with [51, 52]. The CA pattern shows $C_3S$, $C_2S$, $C_4AF$, gypsum and quartz, along with additional phases such as portlandite and calcite in agreement with [53]. The FA contains quartz, mullite and magnetite in agreement with [54], while LS is predominantly composed of calcite and quartz in agreement with [55].

The grain size distribution of sand grading is seen in Table 2. Figure 2 shows the particle size

**Table 1** Compositions of the cement, FA, LS and CA by XRF analysis

| Oxide, weight % | CEM I 42.5 R | CA | FA | LS |
|---|---|---|---|---|
| CaO | 55.63 | 46.16 | 2.22 | 48.02 |
| $SiO_2$ | 14.94 | 12.30 | 36.19 | 3.96 |
| $Al_2O_3$ | 3.37 | 3.07 | 22.66 | 1.59 |
| $Fe_2O_3$ | 4.34 | 1.40 | 15.06 | 1.14 |
| $TiO_2$ | 0.34 | 0.10 | 0.66 | 0.06 |
| $Cr_2O_3$ | 0.02 | 0.02 | 0.01 | 0.00 |
| $Mn_3O_4$ | 0.07 | 0.08 | 0.03 | 0.07 |
| SrO | 0.03 | 0.24 | 0.04 | 0.03 |
| MgO | 1.44 | 4.89 | 0.73 | 0.61 |
| $K_2O$ | 1.53 | 0.79 | 1.78 | 0.32 |
| $Na_2O$ | 0.27 | 1.59 | 0.30 | 0.06 |
| $P_2O_5$ | 0.18 | 0.16 | 0.07 | 0.09 |
| $SO_3$ | 3.94 | 3.41 | 3.22 | 0.18 |
| LOI[a] | 13.91 | 25.80 | 17.02 | 43.88 |
| Total | 100 | 100 | 100 | 100 |

a = loss on ignition

distribution of cement, FA and LS measured with a Malvern Mastersizer 3000 (using a dry chamber, AeroS). The CA is a commercial product and the product datasheet states [56] that it contains: 65–80% of Portland cement (PC) and the rest are hydroxides. Therefore, the refractive index and the absorption index of PC-I were used to estimate its particle size. Although the CA curve distribution is an estimation, it contributes to understanding the effects of CA on the mixtures. Values of $D_{v,10}$, $D_{v,50}$ and $D_{v,90}$ shown in Table 3 indicate that LS exhibits the smallest median particle size ($D_{v,50}$), and FA the largest one.

FTIR spectra (see Fig. S1 of Supplementary Information (S.I.) of cement and CA present bands related to the stretching (1411 $cm^{-1}$ for cement and 1424 $cm^{-1}$ for CA) and bending (874 $cm^{-1}$ for cement and 877 $cm^{-1}$ for CA) vibrations of $CO_3^{2-}$. The bands around 870 $cm^{-1}$ might also be associated with the stretching of S–O bonds in sulfates. The bands at 1104 $cm^{-1}$ for cement and at 1113 $cm^{-1}$ for CA are associated to the symmetric stretching vibrations of S–O presented in the sulfate ion of gypsum. The bands at 916 $cm^{-1}$ and 519 $cm^{-1}$ are associated with asymmetric stretching of Si–O bonds presented in the silicate phase ($C_3S$ and $C_2S$). The spectrum of cement also shows a band at 713 $cm^{-1}$ that is related to the stretching vibrating of Al-O of $C_3A$ in agreement with [58, 59]. The LS spectrum shows bands at 1424 $cm^{-1}$, 873 $cm^{-1}$ and 712 $cm^{-1}$ associated to the stretching vibration and bending vibrations of carbonate, respectively. The band at 1032 $cm^{-1}$ corresponds with asymmetric stretching vibrations Si–O-T (T = Si or Al) in agreement with [60, 61]. In the FA spectrum, the band at 1033 $cm^{-1}$ corresponds with asymmetric stretching vibrations Si–O-T (T = Si or Al) and the band at 667 $cm^{-1}$ is associated with the mullite in agreement with [62].

### 2.3 Grout composition

The experimental program is dedicated to the production of the self-healing grout (grout with CA) and to the production of the reference grout (without CA) as control case with similar workability. The influence of the two most significant parameters (*w*/*b* and *s*/*b* ratios) in the fluidity and bleeding properties was studied. Two different conditions of each parameter were evaluated: *w*/*b* ratio (0.45 and 0.6) and *s*/*b* ratio (0.9 and 1.2). Different approaches were adopted to improve the workability and stability of the mixes: the addition/replacement of cement by FA, addition/replacement of sand by LS and addition of SP. The grouts containing CA were first designed, and then the reference grout. Details of all formulations tested are given in Table 4. After designing each grout, additional tests (setting time, hydration at the early age, rheological behavior and mechanical strength) were carried out to understand the effects of CA on the grout properties.

### 2.4 Mixing procedure

All grouts were prepared in the laboratory using a rotary mixer with a flat beater. All materials were mixed at 24 ± 1 °C. Depending on the composition, the mixture of dry materials varied. FA, SP and defoamer were first mixed with cement for 30 s, the water was then added (mixed for 30s) followed by the addition of fine aggregates. Afterwards, the mixture was mixed for 2 min. For mixtures containing CA and LS, both were previously mixed with sand for 30 s, as recommended by CA manufacturers.

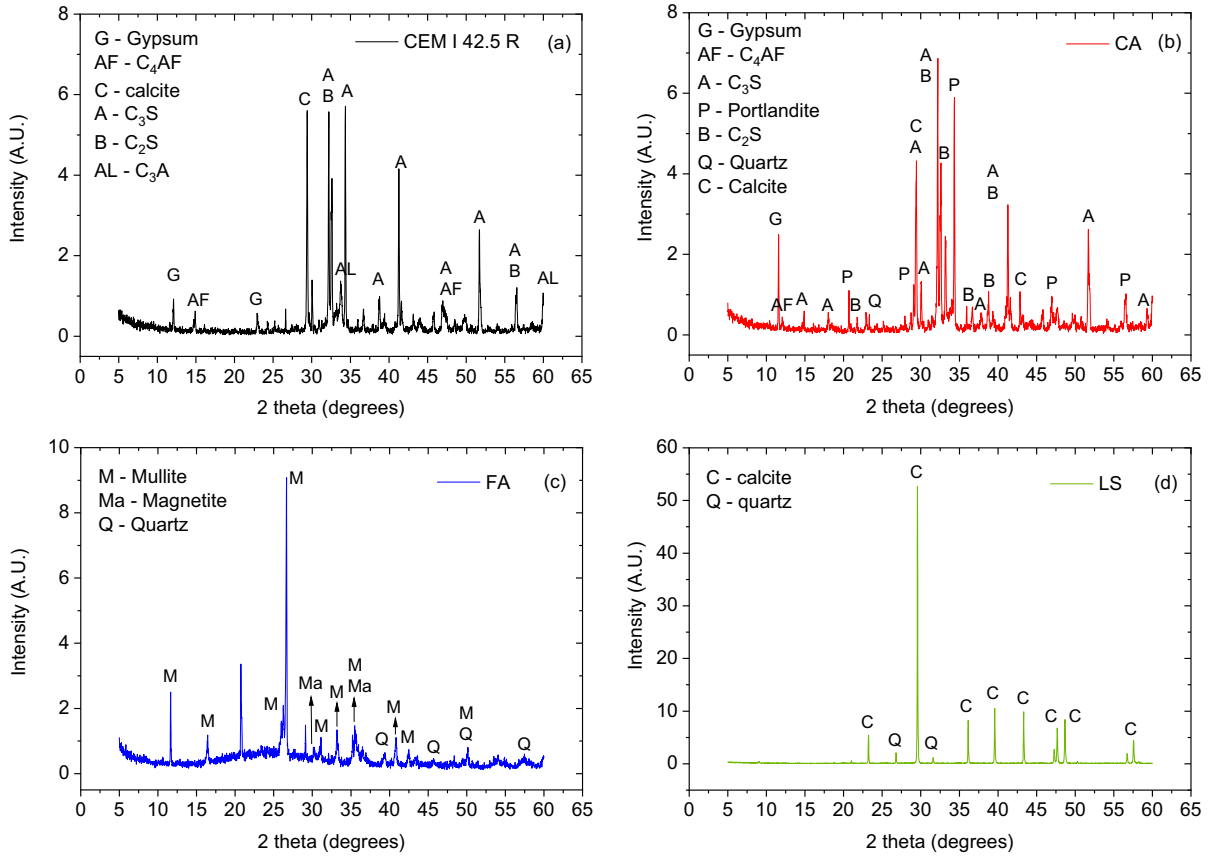


**Fig. 1** XRD pattern of **a** cement, **b** CA, **c** FA and **d** LS

**Table 2** Grain size distribution of sand used for producing grouts [57]

| Merge size (mm) | Lower limit | Intervall average | Upper limit |
|---|---|---|---|
| 2.00 | 0 | 0 | 0 |
| 1.60 | 2 | 7 | 12 |
| 1.00 | 28 | 33 | 38 |
| 0.50 | 62 | 67 | 72 |
| 0.16 | 82 | 87 | 92 |
| 0.08 | 98 | 99 | 100 |

## 2.5 Flow measurements

Fresh grouts were evaluated for flow using a flow table and a flow cone (cone Marsh) as described in [7, 29, 30, 63]. As the consistency can be evaluated by different flow tests, the measurement by the Marsh cone was prioritized over the flow table because in many formulations the spreadability exceeded the diameter of the table. The cone had a nozzle of 11 mm in diameter. The criterion of a continuous flow through the Marsh cone without interruption was adopted to label the grout as "fluid grout". In case that flow could not be measured by the cone, the flow table was used.

## 2.6 Bleeding measurements

In the bleed test, 1000 mL graduated cylinder glass was filled to the 800 mL level. The top of the cylinder was covered to prevent potential evaporation, and it was left to settle. Bleeding was monitored for 3 h. The bleed water was calculated as the water volume released after 3 h divided by the total grout volume (800 mL) and multiplied by 100, as indicated in [64].

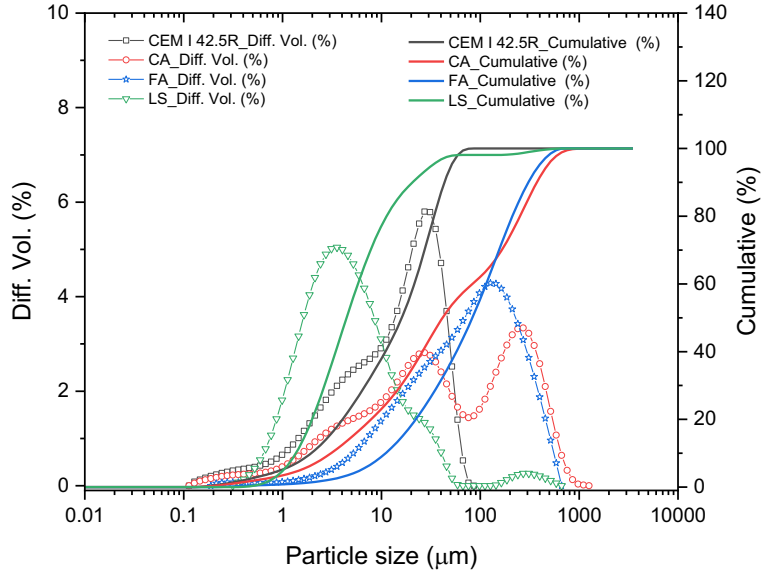


**Fig. 2** Particle size distribution of cement, CA, FA and LS

## 2.7 Setting-time assessment in the early stage

The setting time was evaluated by Vicat needle test and ultrasonic measurements. The initial setting time was measured with an automatic Vicat apparatus (Proeti) according to [65]. Ultrasonic pulse velocity (UPV) was measured with an ultrasonic tester (Pundit 200/Proceq). The pair of transducers (Ø = 50 mm) were placed in a silicon mold (60X60X160 mm) on opposite sides of the specimens at a distance of 16 cm. The ultrasonic frequency of the transducers was 54 kHz and the velocity was measured every 1 min for 21 h.

**Table 3** Dv,10, Dv,50 and Dv,90 of particle size values for cement, CA, FA and LS

| | $D_{v,10}$ (μm) | $D_{v,50}$ (μm) | $D_{v,90}$ (μm) |
|---|---|---|---|
| CEM I 42.5R | 2.0 | 16.1 | 43.5 |
| CA | 3.1 | 41.6 | 374.0 |
| FA | 11.0 | 83.1 | 306.0 |
| LS | 1.4 | 4.4 | 20.6 |

## 2.8 Rheological measurements

A rotational rheometer (Haake Viscotester iQ AIR, ThermoFisher Scientific Haake), equipped with a vane sensor (FL16 4B/SS) and a serrated cup (CC38) was utilized. The torque (up- and down-curves) was measured from 0 to 500 rpm and then decreased from 500 to 0 rpm. Each angular velocity was maintained for the duration of 10 s, so the total measuring time was 280 s (140 s for ascending and 140 s for descending curves). Before any measurement, the samples were pre-sheared at 500 rpm for 60 s, and kept at 0 rpm for 5 s. The data obtained from the rheometer, in relative units (torque and angular velocity), were transformed into fundamental units (shear stress, shear rate and viscosity) following the methodology explained in [66, 67]. Values of A (conversion factor for shear stress) and $M$ (conversion factor for shear rate) of $1.269 \times 10^5$ Pa/Nm and 1.2 (1/s)/(rad/s), respectively, were used for the transformation according to Eq. 4 and 5.

$$\tau = \text{Torque} * A * 10^{-6} \tag{4}$$

$$\dot{\gamma} = \Omega * M \tag{5}$$

where $\tau$ represents the shear stress (Pa), $\dot{\gamma}$ denotes the shear rate ($s^{-1}$) and Ω corresponds to the angular velocity (rad/s), and the torque is expressed in μNm. The measurements were taken at 10, 30 and 60 min after adding water, and they will be named hereafter as t0, t30 and t60. Between each measurement, the grout was kept in the plastic beaker and, before any rheological measurement (at t30 and t60), it was

**Table 4** Grouts mixtures prepared in the study. In all mixes with SP, 0.15% bwoc# of defoamer was added

| | *w/b* | *s/b* | Binder | | Fine aggregates | | CA (%bwob*) | SP (%bwoc#) |
|---|---|---|---|---|---|---|---|---|
| | | | Cement (%bwob*) | FA (%bwob*) | Sand (%bwob*) | LS (%bwob*) | | |
| G1 | 0.45 | 0.9 | 100 | 0 | 100 | 0 | 0 | 0 |
| G2 | 0.45 | 1.2 | 100 | 0 | 100 | 0 | 0 | 0 |
| G3 | 0.6 | 0.9 | 100 | 0 | 100 | 0 | 0 | 0 |
| G4 | 0.6 | 1.2 | 100 | 0 | 100 | 0 | 0 | 0 |
| G5 | 0.45 | 0.9 | 90 | 10 | 100 | 0 | 0 | 0 |
| G6 | 0.45 | 0.9 | 80 | 20 | 100 | 0 | 0 | 0 |
| G7 | 0.45 | 0.9 | 70 | 30 | 100 | 0 | 0 | 0 |
| G8 | 0.6 | 0.9 | 90 | 10 | 100 | 0 | 0 | 0 |
| G9 | 0.6 | 0.9 | 80 | 20 | 100 | 0 | 0 | 0 |
| G10 | 0.6 | 0.9 | 70 | 30 | 100 | 0 | 0 | 0 |
| G11 | 0.45 | 0.9 | 80 | 20 | 100 | 0 | 3 | 0 |
| G12 | 0.45 | 0.9 | 70 | 30 | 100 | 0 | 3 | 0 |
| G13 | 0.45 | 0.9 | 80 | 20 | 100 | 10 | 3 | 0 |
| G14 | 0.4 | 0.9 | 80 | 20 | 90 | 10 | 3 | 0 |
| G15 | 0.45 | 0.9 | 80 | 20 | 100 | 20 | 3 | 0 |
| G16 | 0.45 | 0.9 | 80 | 20 | 80 | 20 | 3 | 0 |
| G17 | 0.45 | 0.9 | 80 | 20 | 100 | 20 | 3 | 2.5 |
| G18 | 0.45 | 0.9 | 80 | 20 | 80 | 20 | 3 | 2.5 |
| G19 | 0.45 | 0.9 | 80 | 20 | 100 | 0 | 0 | 1.0 |
| G20 | 0.45 | 0.9 | 70 | 30 | 100 | 0 | 0 | 1.0 |
| G21 | 0.45 | 0.9 | 70 | 30 | 100 | 0 | 0 | 0.5 |
| G22 | 0.45 | 0.9 | 70 | 30 | 80 | 20 | 0 | 0.5 |
| G23 | 0.45 | 0.9 | 70 | 30 | 85 | 15 | 0 | 0.5 |

* = by weight of binder (bwob) and # = by weight of cement (bwoc)

mechanically stirred at 500 rpm for 5 s and then left for 10 min to stabilize. The Herschel-Bulkley model was used to analyze the down-curves of all flow curves (shear stress vs. shear rate) from 3 to 30 $s^{-1}$ (25–250 rpm) and from 30 to 63 $s^{-1}$ (250–500 rpm).

### 2.9 Hydration at the early stage

The heat of hydration was measured by isothermal calorimetry with a TAM Air 8-channel calorimeter from TA Instruments maintained at 25 °C. The measurements of the grouts (G18 and G23) were carried out using a glass ampoule with automatic stirring. For these measurements all dry components (total mass of 7.68 g respecting the proportion of the components described in Table 4) were mixed together. Once the ampoule was placed inside the calorimeter, water (1.82 g) was added. After adding water, the grout was stirred for two minutes. The heat flow was recorded for 48 h.

The influence on hydration of FA, SP, LS and CA was also evaluated. Polyethylene ampoules containing 5.36 g of dry components and 2.41 g of water were used in this case. The composition of each ampoule is described in Table 5. All dry materials were first mixed manually for 10 s, and then water was added. The mixture was manually mixed for 1 more min. After mixing, the ampoules were placed into the calorimeter. Heat flow began to be recorded after 45 min (when the equipment baseline was stable). The heat flow was recorded for 48 h.

**Table 5** Composition of the cement paste studied in calorimetry tests

| Mixture | *w/b* | Binder | | LS (%bwob*) | CA (%bwob*) | SP (%bwoc#) |
|---|---|---|---|---|---|---|
| | | Cement (%bwob*) | FA (%bwob*) | | | |
| I | 0.45 | 70 | 30 | 0 | 0 | 0 |
| II | 0.45 | 70 | 30 | 0 | 0 | 0.5 |
| III | 0.45 | 70 | 30 | 15 | 0 | 0 |
| IV | 0.45 | 70 | 30 | 15 | 0 | 0.5 |
| V | 0.45 | 80 | 20 | 0 | 0 | 0 |
| VI | 0.45 | 80 | 20 | 0 | 0 | 2.5 |
| VII | 0.45 | 80 | 20 | 20 | 0 | 0 |
| VIII | 0.45 | 80 | 20 | 20 | 0 | 2.5 |
| IX | 0.45 | 80 | 20 | 0 | 3 | 0 |
| X | 0.45 | 80 | 20 | 20 | 3 | 0 |
| XI | 0.45 | 80 | 20 | 0 | 3 | 2.5 |
| XII | 0.45 | 80 | 20 | 20 | 3 | 2.5 |

* = by weight of binder (bwob) and # = by weight of cement (bwoc)

### 2.10 Compressive strength

Compressive strengths were determined after 7, 14 and 28 days of standard curing (temperature at 20 ºC and humidity above 90%), following the standard UNE_EN196-1 [68]. According to the standard, prismatic specimens (40×40×160 mm) were first cast and then broken into two halves by a three-point bending test. Then, on each half, the compressive strength test was carried out with a loading rate of 2400 ± 200 N/s.

## 3 Results/discussion

### 3.1 Design of grout mixtures

The initial tests began with the preparation of grouts containing only cement, sand, water and CA, as summarized in Figs. 3 and 5. The flow and bleeding results were also represented separately and are provided in the S.I. section (Figs. from S2 to S9).

#### *3.1.1 Grout containing CA*

The starting point in the preparation of the grouts was to investigate how the CA would first influence the workability in terms of stability (bleeding measurements) and consistency (flow measurements) of the mixtures. A flowchart illustrating the manufacturing process is presented in Fig. 3.

Figure 3 shows that the increase of water in grouts without CA (G1, G2, G3 and G4 from Fig. S2), produced an increase in fluidity and bleeding. The increase in solids content is an option to minimize bleeding. When increasing the *s/b* of mixtures with *w/b* = 0.45, fluidity and bleeding practically did not change. In turn, for *w/b* = 0.6, fluidity decreased and bleeding increased.

The *w/b* ratio is directly proportional to fluidity, i.e., by increasing the water content, the more fluid the mixture will be. While mixes with *w/b* = 0.45 did not show fluid performance, and only the flow table could be measured, mixes with *w/b* = 0.6 clearly showed a fluid behavior with flow times between 21 – 15 s. However, it was observed for mixtures with *w/b* = 0.6 that the high amount of water destabilized the grout causing segregation and increased bleeding.

Regarding the *s/b* ratio, increasing the *s/b* from 0.9 (G1) to 1.2 (G2) did not improve the workability. For the *w/b* = 0.6 (G3 and G4), the increase of sand amount hindered fluidity and bleeding. Thus, in any case, independently of the *w/b* ratio, no improvement in stability and consistency was observed.

Looking at the results with different *s/b* content, it can be deduced that a *s/b* ratio of 0.9 seemed to be more appropriate for the grout design, since the bleeding results were lower, for both *w/b* ratios evaluated. The best bleeding performance was registered for the mixed with lower *w/b* ratio, although this was not a fluid material.

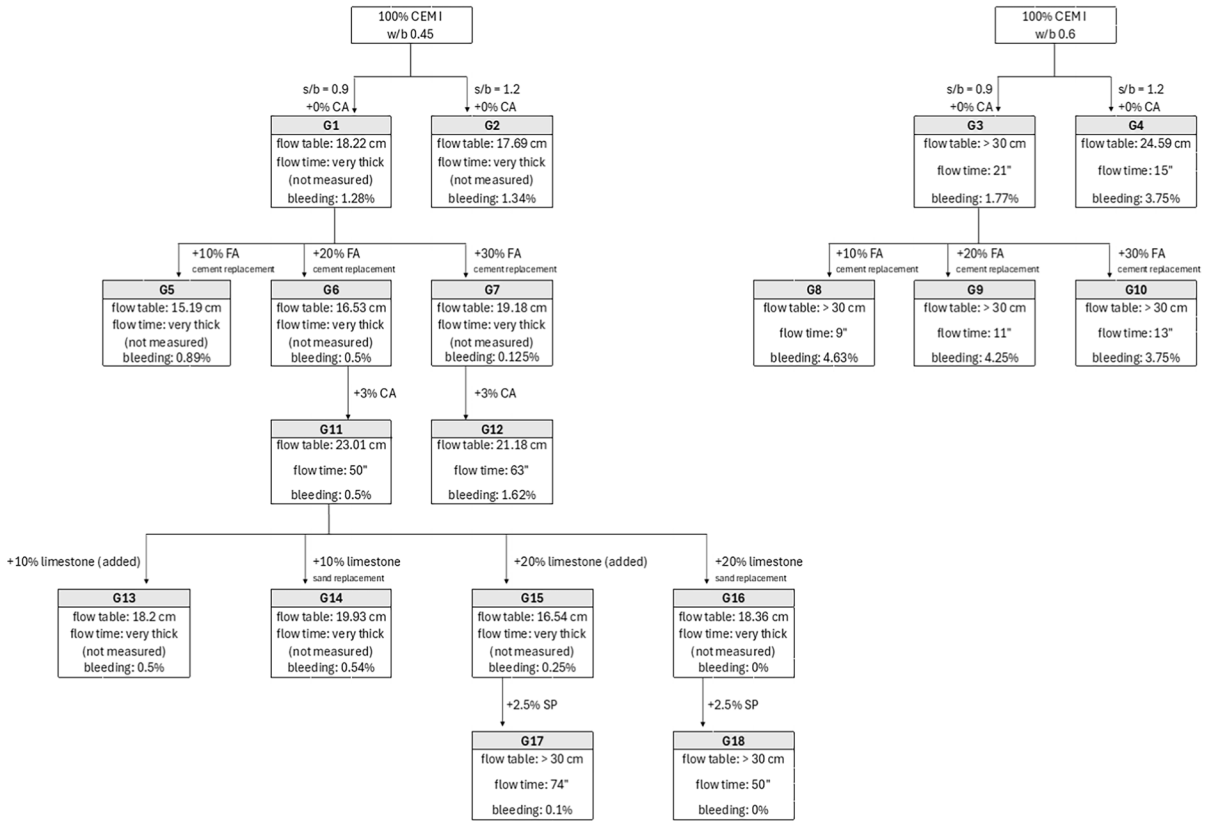


**Fig. 3** Flowchart of the fabrication steps for the cement grout containing CA

To enhance fluidity, 10 wt% to 30 wt% of cement was replaced by FA (Fig. 3, Fig. S3 and Fig. S4). For grout with 30 wt% cement replacement (G7), a slight increase of spreadability was observed. For lower replacements (G5 and G6), flow table values were lower than the grout without FA (G1). The addition of FA within a range of 10–20 wt% did not significantly affect the fluidity of the mixture. However, when the FA content exceeded this range (30 wt%), an increase in fluidity was observed. This behavior can be attributed to the larger particle size of FA (Fig. 2) compared to cement, which would reduce water adsorption and interparticle interactions.

In contrast, for the $w/b = 0.6$, the addition of FA (G8, G9 and G10) caused a decrease in the flow time values in comparison with the mix without FA (G3). As the replacement increased, the flow time tends to increase and bleeding decreases. An increase in fluidity was observed even at the lowest dosage of FA (10 wt%). While the higher water content in these grouts inherently increases fluidity, the introduction of FA at this level reduced the stability of the mixtures, as evidenced by increased bleeding. This behavior is also attributed to particle size and water content. Replacing cement with FA (that has a larger particle size), combined with the presence of larger sand particles, would effectively reduce the surface area and water demand. However, this led to decreased fluidity and greater instability (higher bleeding). Lower bleeding indicates better packing density and grout homogeneity. In this case, the increased bleeding suggests that the solids were not well dispersed and tended to settle slightly. Although mixtures with high $w/b$ (0.6) presented low flow times, the bleeding remained very high.

The slight settling was sufficient to destabilize the mix, increase segregation and therefore affect the workability of the mix. As FA increases, the flow time increases and bleeding decreases. This reduction in workability may be associated with increased

attractive forces between the cement grains and FA particles that were not compensated by the ball bearing effect as also observed by Gullu et al. [34]. They worked with FA having slightly larger particle size than cement and an increase in workability was observed only when replacement exceeded 40% FA. Changes in workability and stability depending on the volume of FA was reported by [69]. Mirza et al. [15] reported that addition of FA with 80% of particles finer than 45 µm resulted in shorter flow times for water/cement ratios between 0.4 and 0.65. Above 0.65, the flow time remained the same, but an increase in bleeding was observed. At low water content, no influence on bleeding was noticed; but w/c ≥ 0.65 favored instability. A great reduction in bleeding was recorded when the same type of FA with larger particle size was used.

The results in Fig. 3 indicated that is preferable to work with $w/b = 0.45$ and $s/b = 0.9$, with FA additions above 20 wt%. Despite not being very fluid, the mixtures are more stable due to their low bleeding. This stability facilitates further optimization of the mixture with the addition of other components.

Before optimizing the mixtures, the CA was added and the results are also presented in Fig. 3 and Fig. S5. The addition of 3 wt% of CA to the grouts G11 and G12 improved the fluidity, but with a greater amount of FA, bleeding increased. A synergic effect appears to occur when CA is combined with 20 wt% FA, maintaining a fluid consistency (continuous flow of the grout through the Marsh Cone in 50 s) with 0.5% of bleeding. As the CA producers do not provide information on the particle size, it is not possible to definitively attribute its effects to particle size alone. However, considering the particle size of the CA assumed in Fig. 2 and the results of G11 and G12, it can be noticed that the particle size of CA is likely larger than that of cement and smaller than that of FA. This assumption is supported by the observed increase in fluidity when CA is added to mixtures containing 20 wt% of FA, without any significant change in bleeding. In contrast, at 30 wt% of FA, fluidity increases, but bleeding is significantly higher.

From G11 to G12 grout, is noticed a reduction in fluidity and an increase in bleeding. This suggests that the smaller particle size of CA likely contributed to an increase in the surface area of the mixture, resulting in higher water absorption and consequently reducing fluidity. Thus, while intermediate particle size of CA appears to improve the balance between fluidity and stability at 20% of FA, its influence becomes more pronounced at higher FA dosage (30% wt), where its interaction with water and other particles affects the overall performance of the mixture.

Considering both results, the mixture G11 (grout with $w/b = 0.45$, $s/b = 0.9$, 3 wt% of CA and with 20 wt% of cement replaced by FA) was selected to be optimized. To reduce bleeding, mineral additions (such as LS) are a possible solution. Thus, two design approaches were used: 1) addition of 10 wt% and 20 wt% of LS in the grout and 2) replacement of sand by LS (10 wt% and 20 wt%).

Comparing the G13, G14, G15 and G16 grouts (Fig. 3 and Fig. S6), a reduction in bleeding is observed, reaching 0.25% and 0% bleeding for the mixes with 20 wt% of filler, as an addition or as a replacement, respectively. The lower the bleeding, the better the packing density and homogeneity of the grout. However, both mixtures showed a decrease in fluidity and none of them could be considered a fluid grout because they remained thick.

It was already expected that fluidity would decrease with the increase of fine particles, but once the bleeding is well controlled, adjusting fluidity by adding SP becomes more manageable. In this way, 2.5 wt% of SP was added into formulations containing 20 wt% of LS (G15 and G16 in Fig. 3 and Fig. S7). Results showed that both mixtures (G17 and G18) presented better flow time, but the mixture replacing sand by LS showed the best fresh properties, with shorter flow time (50 s) and no bleeding. Therefore, this mixture was found to give a good balance between stability and fluidity and was selected (mix G18 in Table 4) as the best formulation for the grout with CA.

### *3.1.2 Reference grout (grout without CA)*

With the aim of evaluating the effect of CA in the cementitious grouts, it was necessary to design a reference grout. The first test was to prepare a grout with the same composition of G18, but without CA. However, a non-stable grout with segregation was obtained (Fig. 4). Then, a new criterion of same fluidity without bleeding was defined as parameter of comparison, even though this reference grout had different composition than the self-healing one containing CA.

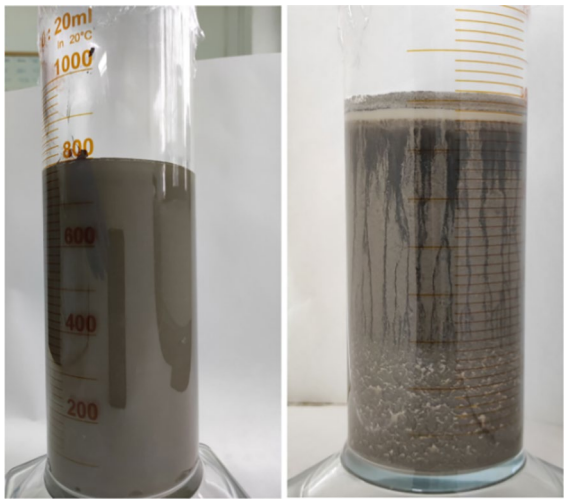


**Fig. 4** Visual appearance of G18 grout with (left) and without (right) the addition of CA

In this way, a reference grout (without CA) was prepared to have the same flow time as the one with CA. To minimize the possible interferences from formulation changes, the new composition was thought to be as close as possible to the G18 grout, which means that the same type of components was maintained, avoiding adding any extra material that had not being used to prepare the G18. Based on the procedure detailed in Fig. 3, the tests started maintaining the same binder composition, the same *s/b* (0.9) and *w/b* (0.45) ratios. The mixtures containing FA (G5, G6 and G7) did not present adequate fluidity but G6 and G7 showed a good bleeding result. Therefore, to improve fluidity, SP was added. A flowchart illustrating the manufacturing process of this new grout is presented in Fig. 5.

The results showed that the addition of 1 wt% of SP (G19 and G20 in Fig. 5 and Fig. S8) improved the fluidity as expected, obtaining a reference grout with a shorter flow time compared to the grout with CA (G18) However, in the G19, the increase in bleed

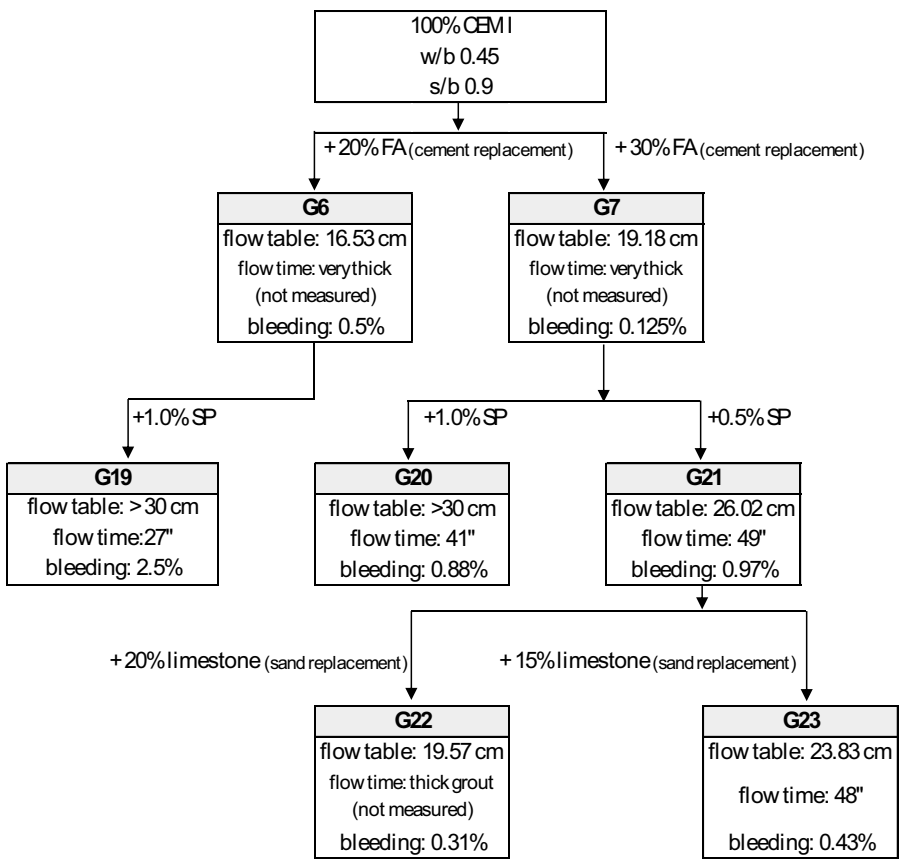


**Fig. 5** The flowchart of the fabrication steps for the reference grout (without CA)

water was more pronounced, leading to destabilization of the mixture and visible segregation. Therefore, the mix with a replacement of 30 wt% (G7) was chosen to be optimized. As 1 wt% of SP decreased the flow time more than expected (G20), another dosage was evaluated: 0.5 wt% (G21). The G20 and G21 showed similar bleeding values, but the flow time of G21 was more similar to that of G18 grout.

To reduce bleeding, LS was added to G21. Trying to not surpass the amount of filler used in G18, the maximum amount tested was 20 wt%. As seen in Fig. 5 and Fig. S9, with 20 wt% (G22), bleeding decreased, but flow worsened. With 15 wt% (G23), the bleeding measured was 0.43% and the flow time continued close to G18. Although zero bleeding was not obtained and, as the criterion of comparison was similar flow time, G23 mixture was selected as reference grout.

## 3.2 Analysis of grout properties

### *3.2.1 Rheological behavior*

From the standpoint of applicability, it is of significant importance to control the rheological behavior of grouts. Fig. S10 (a and b), which is provided as S.I., illustrates the torque versus angular velocity curves at different times (t0, t30 and t60) for G23 and G18. In both cases, by increasing the time, the torque (and consequently, the shear stress and viscosity) increases, as expected.

Figure 6-left and 6-right show the flow curves and viscosity curves, respectively, of G23 and G18 at different times. Although both grouts have the same *w/b* and *s/b* ratios (Table 4), these two grouts display notable distinctions. G18 contains an additional 3 wt% of CA, more FA and LS compared to G23. Consequently, the G18 grout required a higher SP content (2.5 wt%) to achieve the targeted flow time (50 s), which is similar to that of the G23 grout (48 s), as previously discussed. This higher SP amount in G18 would result in improved dispersion, being responsible for the lower viscosity (Fig. 6-right) and yield stress values (Fig. 6-left and Table 6) [70] of G18, at any age, as will be explained below. Furthermore, it is also believed to be responsible for the slower increase in viscosity over time of G18 compared to G23, which is also observed in Fig. 6-right. The effect of SP and CA on the rate of reaction will be examined in greater detail in the following sections.

In general, the grout without CA exhibits shear thinning behavior, which is in accordance with the literature [70]. Moreover, in all cases, at shear rate values lower than 30 $s^{-1}$ (~250 rpm), the viscosity harshly decreases by increasing the shear rate (shear thinning behavior). However, beyond this point, by increasing the shear rate, the viscosity decreases moderately for G23, but it is kept almost constant or slightly increases for G18. This (slight) shear thickening behavior of G18 has also been observed in systems with both high solid loading and superplasticizer content [71]. This variation in viscosity with shear rate (and time) is more clearly discernible in Fig. S11 (provided as S.I.). In this figure, the viscosity values (taken from the down-curves) of both grouts, at selected shear rates, are plotted. All the flow curves (down-curves) were fitted to the Herschel-Bulkley model (Eq. 2), and the obtained rheological parameters are presented Table 6. Here, the fit was adjusted from 3 to 30 $s^{-1}$ and from 30 to 63 $s^{-1}$ due to the differences in the rheological behavior in these ranges of shear rate.

Table 6 shows that the (dynamic) yield stress values of both grouts increase by increasing the hydration time and are lower for G18 than for G23 at any studied time. This is due to the higher SP content in G18, which allows a better dispersion and, hence, lower interaction between particles. Only the yield stress values taken in the adjustment from 3 to 30 $s^{-1}$ have been considered. In addition, G18 presented a lower consistency index, which is a viscosity-related constant, at any studied time than the reference grout. The adjustments are found to fit reasonably well, as evidenced by the high values of r. The lower viscosity (Fig. 6-right) and yield stress (Table 6) values obtained for G18 (at t0) explain its higher slump spread (> 30 cm, Fig. 3) than for G23 (23.8 cm, Fig. 5). The shear thinning behavior of both grouts discussed above (Fig. 6-right) in the range of 3–30 $s^{-1}$, is also corroborated by the Herschel-Bulkley fitting, as values of the exponent, n, lower than 1 were obtained. In contrast, values of $n > 1$ were obtained for G18 in the range from 30 to 63 $s^{-1}$, confirming the (slight) shear thickening behavior previously described. These results contribute to the understanding of the rheological behavior of both grouts under different hydration times and stirring conditions.

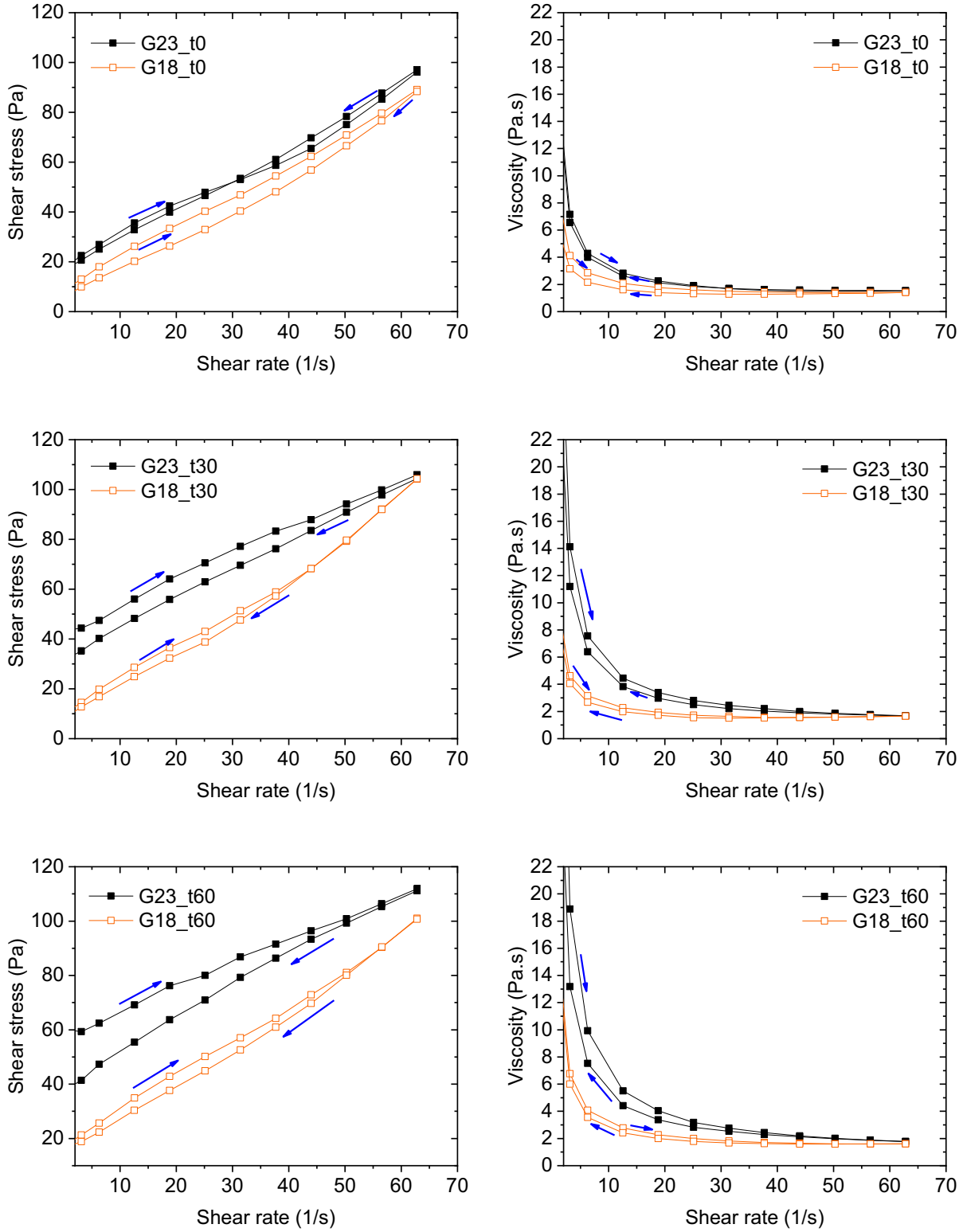


**Fig. 6** Flow curves (left) and viscosity curves (right) of fresh grouts without and with CA at different times (t0, t30, t60)

**Table 6** Values of yield stress, consistency index and flow behavior index (exponent) obtained using the Herschel-Bulkley model (from 3 to 30 s-1 and from 30 to 63 s-1, using the down-curves) for G23 and G18 grouts

| | Shear rate range ($s^{-1}$) | Time | Yield stress (Pa) | *K* (Consistency index, Pa $s^n$) | *n* (exponent) | *r* |
|---|---|---|---|---|---|---|
| G23 (0% CA) | From 3 to 30 | $t_0$ | 14.78 | 2.29 | 0.82 | 1.0000 |
| | | t30 | 28.90 | 2.54 | 0.81 | 0.9999 |
| | | t60 | 33.99 | 3.18 | 0.76 | 0.9997 |
| | From 30 to 63 | t0 | - | 0.27 | 1.35 | 1.0000 |
| | | t30 | - | 1.53 | 0.94 | 0.9999 |
| | | t60 | - | 7.61 | 0.60 | 0.9999 |
| G18 (3% CA) | From 3 to 30 | t0 | 6.24 | 1.26 | 0.94 | 0.9999 |
| | | t30 | 7.09 | 2.13 | 0.94 | 0.9999 |
| | | t60 | 14.62 | 1.37 | 0.96 | 0.9995 |
| | From 30 to 63 | t0 | - | 0.06 | 1.71 | 0.9999 |
| | | t30 | - | 0.23 | 1.44 | 1.0000 |
| | | t60 | - | 0.20 | 1.44 | 0.9999 |

### *3.2.2 Hydration at the early stage*

Figure 7 shows the rate of heat development and cumulative heat generated in the binder hydration of each grout during the first 48 h. Common heat release curves with three main stages (initial dissolution, induction and main reaction stage) are observed in Fig. 7a. During the initial dissolution stage (from 0 to 0.2 h), it can be observed that the grout with CA (G18) released more heat than the reference grout (G23) with longer induction period for the grout with CA (from 0.2 to 6 h) than for the reference (from 0.2 to 4 h). The main differences are observed at the main reaction period, when the large-scale nucleation and growth of reaction products occur. The reference grout reaches a heat peak between 8 −10 h, whereas the peak of grout containing CA appears between 12 −14 h. The cumulative heat of the grout with CA is slightly lower than that of the reference (Fig. 7b). These results are consistent with the relative binder hydration rates discussed above.

As the cement hydration depends on the chemical interaction between the different components of the mixture, the effect of FA, SP, LS and CA in the cement pastes was also monitored through calorimetry, and the results are presented in Fig. 8.

Figure 8a shows that FA does not significantly affect the heat release during the acceleration period. However, with LS additions, hydration reactions are slightly advanced and a shoulder appears after 16 h

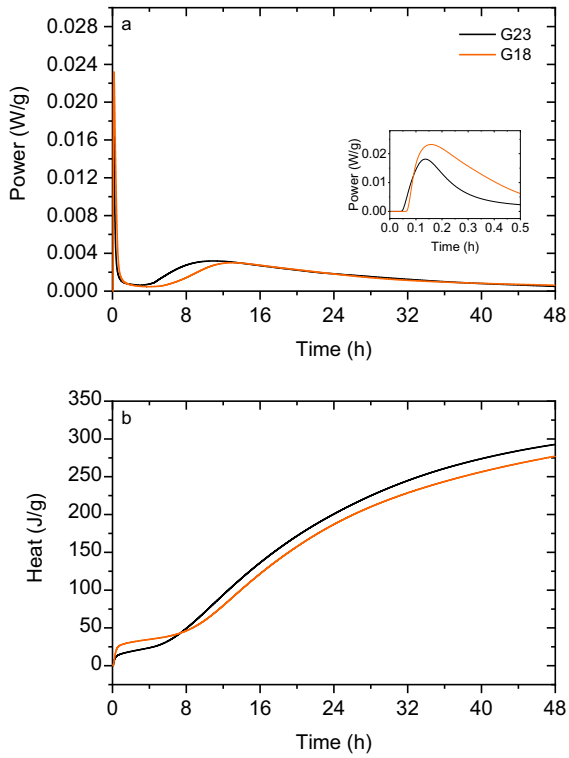


**Fig. 7** Calorimetry curves for first 48 h of G23 (0% CA) and G18 (3%CA) mixtures: **a** rate of heat evolution and (b) cumulative heat evolution per gram of cement

(which can be associated with the formation of $C_3A$ hydrates promoted by LS). This effect is more pronounced in the G18 paste. LS is reported to delay setting by suppressing $C_3A$ reactions through the formation of calcium carboaluminate [72]. The cumulative heat remains similar between the pastes, indicating no significant difference in total heat released.

The effect of SP is illustrated in Fig. 8b, c. SP generally delays the main reaction period [69]. In G23 (Fig. 8b), the low dosage of SP (0.5 wt%) does not seem to have a significant impact on early hydration, as similar curves are observed. When combined with LS, SP slightly extends the induction period and accentuates the shoulder. At a higher SP dosage (2.5 wt%), as in G18 (Fig. 8c), the onset of heat release is delayed by almost 5 h and the cumulative heat evolution is reduced. In the presence of LS, SP further delays the acceleration period, the shoulder remains unchanged and cumulative heat decreases.

Figure 8d highlights the influence of CA in the binder G18 (green curve). CA shortens the dormant period and increases heat release, particularly during $C_3S$ hydration and shoulder formation. When combined with LS (yellow curve), CA accelerates the formation of monosulfate, as the shoulder appears around 14 h. However, the cumulative heat is lower than the paste without LS but slightly higher than paste with LS only (Fig. 8c—green curve).

With 2.5 wt% SP added to the binder G18 containing CA (Fig. 8d—grey curve), the SP extends the induction period but reduces the heat-flow peak associated with $C_3S$ hydration. The shoulder linked to $C_3A$ hydrates is absent, indicating SP interferes with the contribution of CA. In the paste with LS + CA (blue curve), SP extends the induction period without reducing the heat-flow peak. Compared to the paste without LS (yellow curve), LS seems to contribute to this delay as the acceleration phase begins slightly later. No significant change in $C_3A$ dissolution (shoulder shape or heat released) is observed, and the cumulative heat is similar to that of the of the paste containing only CA + SP (grey curve).

#### *3.2.3 Initial setting-time assessment in the early stage*

Figure 9 shows the development of the resistance to the penetration of Vicat needle and the changes on pulse velocity over time. A typical three-stage evolution of pulse velocity on the first day was registered: a low propagation velocity for a long initial period (first stage), followed by a sudden increase in velocity as hardening begins to occur (second stage) and then a more gradual increase in velocity (third stage). The initial setting time, determined through UPV measurements, was considered as the first moment the pulse-wave begins to increase [73]. A clear delay in the initial setting time is observed for G18. However, once the formation of the first hydrates begins, a faster development can be deduced from the pulse-wave velocity if compared with the reference grout.

Comparing with the initial setting time, we observe that they were quite similar as the sudden increase in pulse velocity occurred at very similar times to the development of penetration resistance. Similar good correlations between the evolution of cement hydration and the initial curing time were also reported by other authors [74–76].

Grout containing CA (G18) has a longer initial setting time, almost 4 h longer than the reference grout (G23). This retarding effect may be mainly related to the amount of the SP used, as this grout contains 5 times more SP. It was observed from the calorimetry measurements that the addition of 0.5 wt% of SP to G23 did not affect the dormant period nor the hydration processes of the mix.

Similarly done in calorimetry measurements, the effect of each component on G18 mixture was also analyzed. Figure 10 shows that CA accelerates the initial setting (peak appears almost 1 h before the reference peak) while SP delays it (peak appears approximately after 6.5 h later than the reference peak). Once combined, setting begins 1 h earlier than the mixture containing only SP. These results agree with those presented in Fig. 8, as calorimetry measurements also indicated the same trend of each component.

#### *3.2.4 Compressive strength*

The compressive strengths of grouts cured at different ages are shown in Fig. 11, where can be seen that the strength of both increases over time. The strength of the grout with CA (G18) is greater at any age, which suggests that the addition of CA did not negatively impact the mechanical strength. In fact, it promoted microstructural changes that contributed to the strength gain. Additionally, the higher filler content

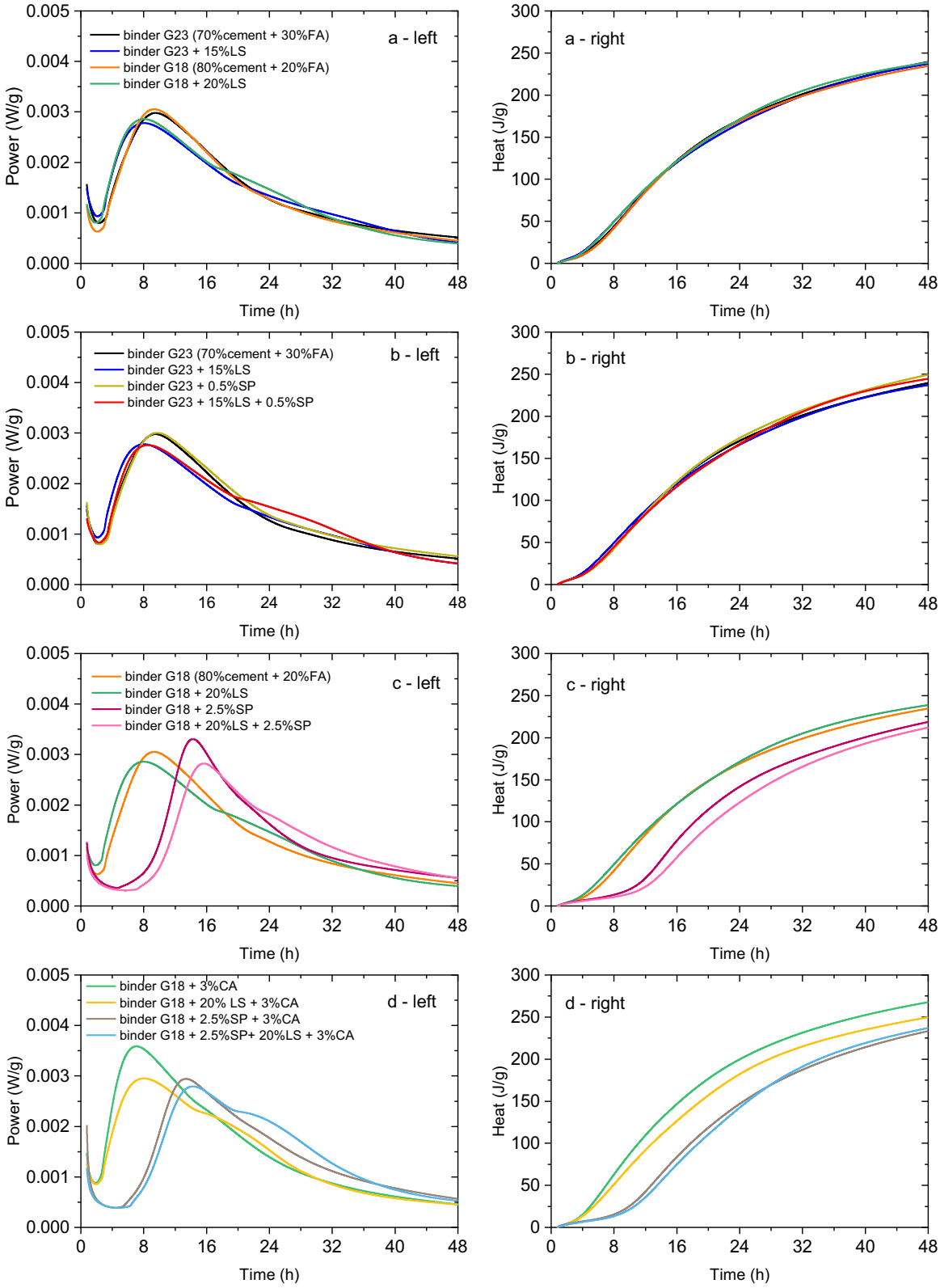
a - left
binder G23 (70%cement + 30%FA)
binder G23 + 15%LS
binder G18 (80%cement + 20%FA)
binder G18 + 20%LS
Power (W/g)
Time (h)
a - right
Heat (J/g)
Time (h)
b - left
binder G23 (70%cement + 30%FA)
binder G23 + 15%LS
binder G23 + 0.5%SP
binder G23 + 15%LS + 0.5%SP
Power (W/g)
Time (h)
b - right
Heat (J/g)
Time (h)
c - left
binder G18 (80%cement + 20%FA)
binder G18 + 20%LS
binder G18 + 2.5%SP
binder G18 + 20%LS + 2.5%SP
Power (W/g)
Time (h)
c - right
Heat (J/g)
Time (h)
d - left
binder G18 + 3%CA
binder G18 + 20% LS + 3%CA
binder G18 + 2.5%SP + 3%CA
binder G18 + 2.5%SP+ 20%LS + 3%CA
Power (W/g)
Time (h)
d - right
Heat (J/g)
Time (h)

◂**Fig. 8** Heat flux (per gram of cement) of pastes with amounts of FA, LS, SP and CA: rate of heat evolution (left) and cumulative heat evolution (right)

in G18 also contributed to creating a more compact structure by filling the pores, further enhancing its mechanical performance through the pore-filling effect.

## 4 Conclusions

The paper focused on the design process of a grout with (G18) and without CA (G23) and the effect of this admixture could cause on the grout properties. Although G18 and G23 have similar flow time, their performance changed due to differences in composition and particle interactions.

In terms of fresh-state behavior, the addition of CA consistently altered particle dispersion, absorbing more water, affecting the stability and consistency of the grout. While CA reduced bleeding, higher dosages of SP were necessary to obtain a good fluidity. Moreover, the additions of FA and LS influenced the particle packing, directly impacting the mechanical strength and early-age hydration of the grouts.

The grout with CA also exhibited lower viscosity, but this effect was mainly due to the significantly higher SP dosage rather than the presence of CA. The influence of CA on fresh properties was secondary to the effects of SP.

Small changes in components induced significant variations in workability, emphasizing the critical importance of parameters such as the w/c ratio, *s*/*b* ratio and overall composition. The characterization results did not highlight any significant effects solely attributable to the presence of CA, as other parameters played more decisive roles in shaping the final properties.

The varying outcomes reinforce the critical need to tailor grout design to the specific requirements of the site or structure to be grouted. A one-size-fits-all approach is inadequate, as each formulation responded uniquely to variations in the *w*/*b* and *s*/*b* ratios, SP dosage, and the additions of SCM and CA.

Although the sole effect of CA could not be fully quantified, the design process allows other workers/

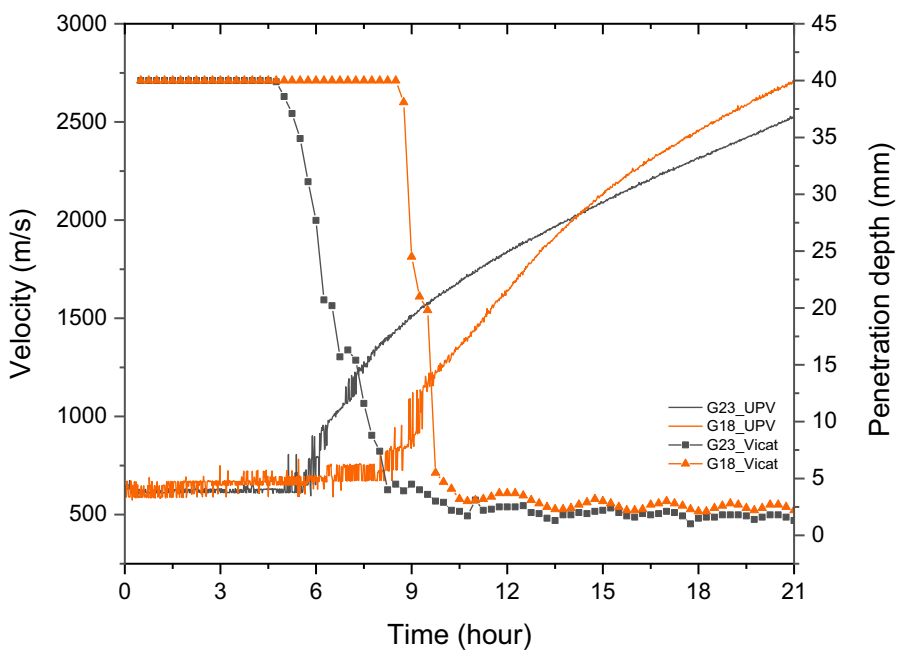


**Fig. 9** Evolution of UPV and development of penetration resistance

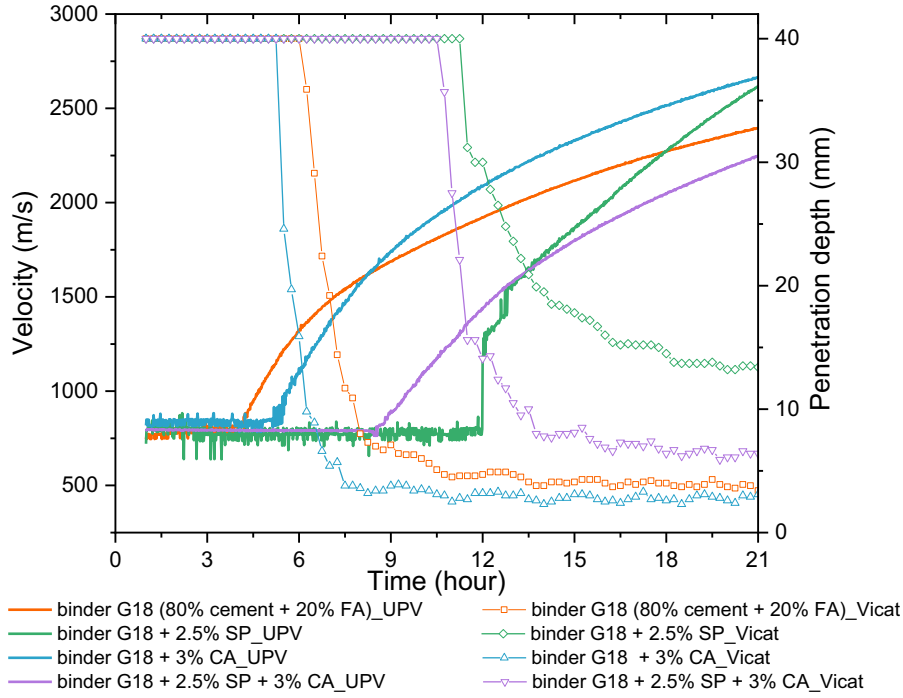


**Fig. 10** Effect of SP and CA on the initial setting time of the binder used in the preparation of grout with CA (G18)

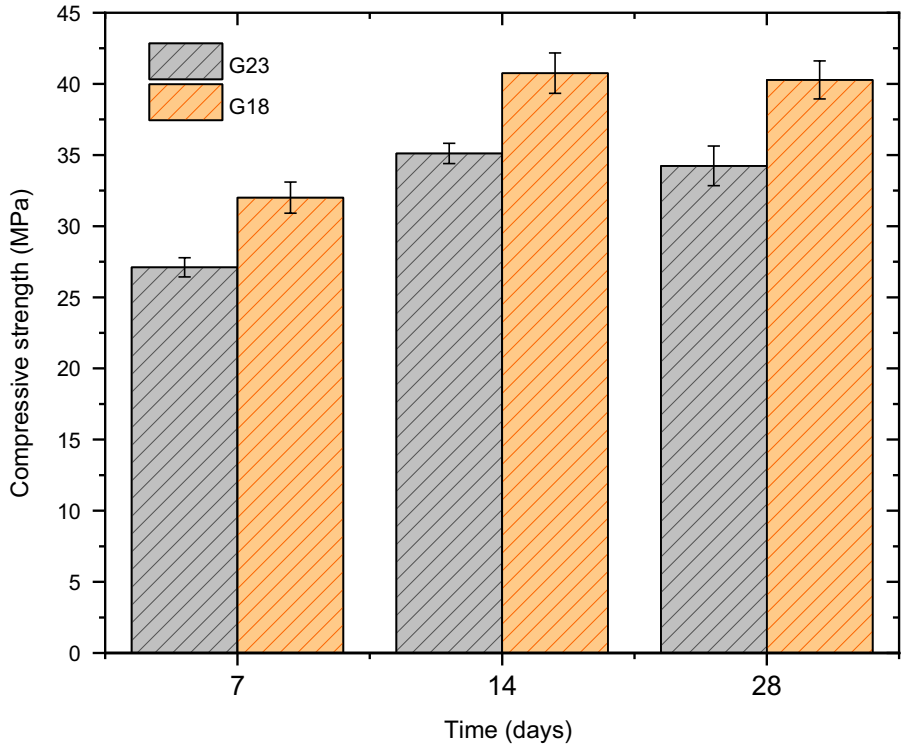


**Fig. 11** Compressive strength of grouts at 7, 14 and 28 days

researchers to compare and identify gaps and potential improvements to make performance comparable.

**Funding** Funding for open access publishing: Universidad de Córdoba/CBUA. This project has received funding from the European Union's Horizon 2020 research and innovation programme under the Marie Skłodowska-Curie grant agreement No 860006. The authors also thank Enrico Gastaldo, from*Penetron Italia Srl, for providing the Penetron Admix,Master Builders Solutions(Sandro Moro and Pere Borralleras) for supplying the MasterCast 228 and defoamer andCemento Cosmos S.A.for supplying the cement and LS.*

**Declarations**

**Competing interests** The authors report there are no competing interests to declare.



## References

1. da Rocha Gomes S, Ferrara L, Sánchez L, Moreno MS (2023) A comprehensive review of cementitious grouts: composition, properties, requirements and advanced performance. Constr Build Mater 375:1–16. https://doi.org/10.1016/j.conbuildmat.2023.130991
2. Tattersall GH (1991) Workability and quality control of concrete, 1st Edition. Taylor & Francis Group, LLC, London
3. Neville AM, Brooks JJ (2010) Concrete technology, 2nd ed. Pearson Education Limited
4. Hamilton HRT, Alvarez GA, Sessions L (2002) Post-Tensioning Grout Bleed, Duct, And Anchorage Protection Test Principal Investigator: BC354 RPWO #73 4. Title and Subtitle 5. Report Date Post-Tensioning Grout Bleed, Duct, and Anchorage Protection Test
5. ASTM C938 (2005) Standard practice for proportioning grout mixtures for preplaced-aggregate concrete. American Society of Testing and Materials 80:1–4
6. Plotkin S, Sessions L, Edwards D (2002) Grouting of bridge post-tensioning tendons
7. ASTM C1107 (2020) Standard specification for packaged dry, hydraulic-cement grout (Nonshrink). ASTM International
8. Sha F, Li S, Liu R et al (2019) Performance of typical cement suspension-sodium silicate double slurry grout. Constr Build Mater 200:408–419. https://doi.org/10.1016/j.conbuildmat.2018.12.119
9. Sha F, Lin C, Li Z, Liu R (2019) Reinforcement simulation of water-rich and broken rock with Portland cement-based grout. Constr Build Mater 221:292–300. https://doi.org/10.1016/j.conbuildmat.2019.06.094
10. Peng Y, Lauten RA, Reknes K, Jacobsen S (2017) Bleeding and sedimentation of cement paste measured by hydrostatic pressure and Turbiscan. Cem Concr Compos 76:25–38. https://doi.org/10.1016/j.cemconcomp.2016.11.013
11. Johnson D (1999) Cementitious grouts - standards update 1999. In: Specialist techniques and materials for concrete construction. Thomas Telford Publishing, pp 41–48
12. Erdem TK, Bilgiç E, Kanpara Cıvaş Z (2019) A new method to quantify the robustness of self-consolidating grouts. Constr Build Mater. https://doi.org/10.1016/j.conbuildmat.2019.116849
13. Lombardi G (1985) The role of cohesion in cement grouting of rock. In: Quinzième congrès international des grands barrages. Lausanne, Switzerland, pp 235–261
14. Azadi MR, Taghichian A, Taheri A (2017) Optimization of cement-based grouts using chemical additives. J Rock Mech Geotech Eng 9:623–637. https://doi.org/10.1016/j.jrmge.2016.11.013
15. Mirza J, Mirza MS, Roy V, Saleh K (2002) Basic rheological and mechanical properties of high-volume fly ash grouts. Constr Build Mater 16:353–363. https://doi.org/10.1016/S0950-0618(02)00026-0
16. Perez-Garcia F, Parron-Rubio ME, Garcia-Manrique JM, Rubio-Cintas MD (2019) Study of the suitability of different types of slag and its influence on the quality of green grouts obtained by partial replacement of cement. Materials. https://doi.org/10.3390/ma12071166
17. Shamsuddoha M, Hüsken G, Schmidt W et al (2018) Ternary mix design of grout material for structural repair using statistical tools. Constr Build Mater 189:170–180. https://doi.org/10.1016/j.conbuildmat.2018.08.156
18. Şahmaran M, Özkan N, Keskin SB et al (2008) Evaluation of natural zeolite as a viscosity-modifying agent for cement-based grouts. Cem Concr Res 38:930–937. https://doi.org/10.1016/j.cemconres.2008.03.007
19. Li S, Zhang J, Li Z et al (2019) Investigation and practical application of a new cementitious anti-washout grouting material. Constr Build Mater 224:66–77. https://doi.org/10.1016/j.conbuildmat.2019.07.057
20. Krishnamoorthy TS, Gopalakrishnan S, Balasubramanian K et al (2002) Investigations on the cementitious grouts containing supplementary cementitious materials. Cem Concr Res 32:1395–1405. https://doi.org/10.1016/S0008-8846(02)00799-8
21. Lothenbach B, Scrivener K, Hooton RD (2011) Supplementary cementitious materials. Cem Concr Res 41:1244–1256. https://doi.org/10.1016/j.cemconres.2010.12.001
22. Snellings R, Mertens G, Elsen J (2012) Supplementary cementitious materials. Rev Mineral Geochem 74:211–278. https://doi.org/10.2138/rmg.2012.74.6

23. Felekoğlu B, Tosun K, Baradan B et al (2006) The effect of fly ash and limestone fillers on the viscosity and compressive strength of self-compacting repair mortars. Cem Concr Res 36:1719–1726. https://doi.org/10.1016/j.cemconres.2006.04.002
24. Bentz DP, Ferraris CF, Galler MA et al (2012) Influence of particle size distributions on yield stress and viscosity of cement-fly ash pastes. Cem Concr Res 42:404–409. https://doi.org/10.1016/j.cemconres.2011.11.006
25. Zhang S, Qiao WG, Chen PC, Xi K (2019) Rheological and mechanical properties of microfine-cement-based grouts mixed with microfine fly ash, colloidal nanosilica and superplasticizer. Constr Build Mater 212:10–18. https://doi.org/10.1016/j.conbuildmat.2019.03.314
26. Péra J, Husson S, Guilhot B (1999) Influence of finely ground limestone on cement hydration. Cem Concr Compos 21:99–105. https://doi.org/10.1016/S0958-9465(98)00020-1
27. Ye G, Liu X, De Schutter G et al (2007) Influence of limestone powder used as filler in SCC on hydration and microstructure of cement pastes. Cem Concr Compos 29:94–102. https://doi.org/10.1016/j.cemconcomp.2006.09.003
28. Li Y, Zhang G, Jiang H et al (2020) Performance assessment of a newly developed and highly stable sandy cementitious grout for karst aquifers in China. Environ Earth Sci. https://doi.org/10.1007/s12665-020-8894-8
29. ASTM C230 (2020) Standard specification for flow table for use in tests of hydraulic cement. ASTM International https://doi.org/10.1520/C0230
30. ASTM C939 (2016) Standard test method for flow of grout for preplaced-aggregate concrete (flow cone method). ASTM International. https://doi.org/10.1520/C0939-16A
31. American Concrete Institute (2013) ACI CT-13. ACI concrete terminology - An ACI Standard
32. Zhou Z, Zang H, Zhang J et al (2018) Filtration behaviour of cement-based grout in porous media. Transp Porous Media 125:435–463. https://doi.org/10.1007/s11242-018-1127-x
33. Vance K, Sant G, Neithalath N (2015) The rheology of cementitious suspensions: a closer look at experimental parameters and property determination using common rheological models. Cem Concr Compos 59:38–48. https://doi.org/10.1016/j.cemconcomp.2015.03.001
34. Güllü H, Cevik A, Al-Ezzi KMA, Gülsan ME (2019) On the rheology of using geopolymer for grouting: a comparative study with cement-based grout included fly ash and cold bonded fly ash. Constr Build Mater 196:594–610. https://doi.org/10.1016/j.conbuildmat.2018.11.140
35. Vasumithran M, Anand KB, Sathyan D (2020) Effects of fillers on the properties of cement grouts. Constr Build Mater. https://doi.org/10.1016/j.conbuildmat.2020.118346
36. Liu J, Li Y, Zhang G, Liu Y (2019) Effects of cementitious grout components on rheological properties. Constr Build Mater. https://doi.org/10.1016/j.conbuildmat.2019.08.035
37. Rumman R, Bediwy A, Alam MS (2024) Revolutionizing concrete durability: case studies on encapsulation- based chemical (autonomous) self-healing techniques and future directions—a critical review. Case Stud Constr Mater. https://doi.org/10.1016/j.cscm.2024.e03216
38. Ghosh SK (2009) Self-healing materials: fundamentals, design strategies, and applications. WILEY-VCH Verlag GmbH & Co, KGaA, Germany
39. Petrucci RDS, Hastenpflug D (2017) Evaluation of crystalline waterproofing admixture on portland cement concrete. In: Proceedings of international structural engineering and construction
40. Cappellesso VG, Van Mullem T, Gruyaert E et al (2024) Self-healing concrete with a bacteria-based or crystalline admixture as healing agent to prevent chloride ingress and corrosion in a marine environment. Dev Built Environ 19:100486. https://doi.org/10.1016/j.dibe.2024.100486
41. Sisomphon K, Copuroglu O, Koenders EAB (2012) Self-healing of surface cracks in mortars with expansive additive and crystalline additive. Cem Concr Compos 34:566–574. https://doi.org/10.1016/j.cemconcomp.2012.01.005
42. Ferrara L, Krelani V, Moretti F (2016) On the use of crystalline admixtures in cement based construction materials: from porosity reducers to promoters of self healing. Smart Mater Struct 25:1–17. https://doi.org/10.1088/0964-1726/25/8/084002
43. de Oliveira A, S, Dweck J, Fairbain E de MR, Filho ORDT, (2020) Crystalline admixture effects on crystal formation phenomena during cement pastes' hydration. J Therm Anal Calorim 139:3361–3375. https://doi.org/10.1007/s10973-019-08745-0
44. American Concrete Institute Committee 212 (2017) ACI 212.3R-10 Report on Chemical Admixtures for concrete_Chapter 15
45. Michael J, Smith SH, Durham SA, Chorzepa MG (2018) Crack control in concrete walls through novel mixture design, full-scale testing, and finite element analysis. Constr Build Mater 166:301–314. https://doi.org/10.1016/j.conbuildmat.2018.01.081
46. Roig-Flores M, Pirritano F, Serna P, Ferrara L (2016) Effect of crystalline admixtures on the self-healing capability of early-age concrete studied by means of permeability and crack closing tests. Constr Build Mater 114:447–457. https://doi.org/10.1016/j.conbuildmat.2016.03.196
47. Neverkovica D, Korjakins A (2015) Influence of additives on reinforced concrete durability. Constr Sci 16:21–26. https://doi.org/10.1515/cons-2014-0009
48. de Oliveira A, S, Gomes O da FM, Ferrara L, et al (2021) An overview of a twofold effect of crystalline admixtures in cement-based materials: from permeability-reducers to self-healing stimulators. J Build Eng 41:102400. https://doi.org/10.1016/j.jobe.2021.102400
49. Wang L, Zhang G, Wang P, Yu S (2018) Effects of fly ash and crystalline additive on mechanical properties of two-graded roller compacted concrete in a high RCC arch dam. Constr Build Mater 182:682–690. https://doi.org/10.1016/j.conbuildmat.2018.06.101
50. Zheng K, Yang X, Chen R, Xu L (2019) Application of a capillary crystalline material to enhance cement grout for sealing tunnel leakage. Constr Build Mater 214:497–505. https://doi.org/10.1016/j.conbuildmat.2019.04.095

51. Aïtcin PC (2016) Supplementary cementitious materials and blended cements. In: Science and technology of concrete admixtures. Elsevier Ltd, pp 53–73
52. Szeląg M (2018) Influence of specimen's shape and size on the thermal cracks' geometry of cement paste. Constr Build Mater 189:1155–1172. https://doi.org/10.1016/j.conbuildmat.2018.09.078
53. Nasim M, Dewangan UK, Deo SV (2020) Autonomous healing in concrete by crystalline admixture: a review. Mater Today Proc 32:638–644. https://doi.org/10.1016/j.matpr.2020.03.116
54. Park B, Choi YC (2021) Self-healing products of cement pastes with supplementary cementitious materials, calcium sulfoaluminate and crystalline admixtures. Materials. https://doi.org/10.3390/ma14237201
55. Kamitsou MD, Kanellopoulou DG, Christogerou A et al (2020) Valorization of FGD and bauxite residue in sulfobelite cement production. Waste Biomass Valoriz 11:5445–5456. https://doi.org/10.1007/s12649-020-01055-9
56. Penetron Penetron Admix datasheet. https://www.penetron.es/products/PENETRON-ADMIX/. Accessed 23 Jan 2025
57. Normensand sand granulometry_Normensand. https://www.normensand.de/en/products/cen-standard-sand-en-196-1/. Accessed 23 Jan 2025
58. Mohammadreza Hassani E, Vessalas K, Sirivivatnanon V, Baweja D (2017) Influence of permeability-reducing admixtures on water penetration in concrete. ACI Mater J 114:911–922. https://doi.org/10.14359/51701002
59. Menezes RMRO, Costa LM, Tavares LRC et al (2020) Effect of water content and particle size on the thermal decomposition of ground cement paste. Revista Materia. https://doi.org/10.1590/s1517-707620200001.0888
60. Robert M. Silverstein, Francis X. Webster DJK (2005) Spectrometric identification of organic compounds, 7th ed. John Wiley & Sons, Inc.
61. Akbar NA, Aziz HA, Adlan MN (2021) The characteristics of limestone and anthracite coal as filter media in treating pollutants from groundwater. Int J Environ Sci Dev 12:58–62. https://doi.org/10.18178/IJESD.2021.12.2.1318
62. Darmayanti L, Notodarmojo S, Damanhuri E et al (2019) Preparation of alkali-activated fly ash-based geopolymer and their application in the adsorption of copper (II) and zinc (II) ions. MATEC Web Conf 276:06012. https://doi.org/10.1051/matecconf/201927606012
63. C1437 A (2001) Standard test method for flow of hydraulic cement mortar. ASTM International
64. ASTM C940 (2010) Standard test method for expansion and bleeding of freshly mixed grouts for preplaced-aggregate concrete in the laboratory. ASTM International
65. 480-2 U-E (2007) Admixtures for concrete, mortar and grout part 2: determination of setting time
66. Tattersall GH, Banfill PFG (1983) The rheology of fresh concrete. Pitman Advanced Pub. Program, London, UK
67. Flatt RJ, Larosa D, Roussel N (2006) Linking yield stress measurements: spread test versus Viskomat. Cem Concr Res 36:99–109. https://doi.org/10.1016/j.cemconres.2005.08.001
68. UNE-EN 196-1 (2005) Methods of testing cement. Part 1: determination of strength
69. García-Maté M, De La Torre AG, León-Reina L et al (2013) Hydration studies of calcium sulfoaluminate cements blended with fly ash. Cem Concr Res 54:12–20. https://doi.org/10.1016/j.cemconres.2013.07.010
70. Nguyen VH, Remond S, Gallias JL (2011) Influence of cement grouts composition on the rheological behaviour. Cem Concr Res 41:292–300. https://doi.org/10.1016/j.cemconres.2010.11.015
71. Sanfelix SG, Santacruz I, Szczotok AM et al (2019) Effect of microencapsulated phase change materials on the flow behavior of cement composites. Constr Build Mater 202:353–362. https://doi.org/10.1016/j.conbuildmat.2018.12.215
72. Feldman RF, Ramachandran VS, Sereda PJ (1965) Influence of CaCO3 on the hydration of 3CaO·Al2O3. J Am Ceram Soc 48:25–30. https://doi.org/10.1111/j.1151-2916.1965.tb11787.x
73. Zhang Y, Zhang W, She W et al (2012) Ultrasound monitoring of setting and hardening process of ultra-high performance cementitious materials. NDT E Int 47:177–184. https://doi.org/10.1016/j.ndteint.2009.10.006
74. Von Daake H, Stephan D (2016) Setting of cement with controlled superplasticizer addition monitored by ultrasonic measurements and calorimetry. Cem Concr Compos 66:24–37. https://doi.org/10.1016/j.cemconcomp.2015.11.004
75. Yoo DY, Shin HO, Yoon YS (2016) Ultrasonic monitoring of setting and strength development of ultra-high-performance concrete. Materials. https://doi.org/10.3390/ma9040294
76. Trtnik G, Turk G, Kavčič F, Bosiljkov VB (2008) Possibilities of using the ultrasonic wave transmission method to estimate initial setting time of cement paste. Cem Concr Res 38:1336–1342. https://doi.org/10.1016/j.cemconres.2008.08.003